Proceedings of the 21st ICSMGE, Vienna, Austria, 14 – 19 June 2026. Pistrol, Adam & Schweiger (eds.)
Published by: ÖGG, Austrian Society for Geomechanics, Salzburg, Austria, ISBN 978-3-9503898-4-5
https://doi.org/10.53243/ICSMGE2026-731

One century with Mononobe–Okabe method: Seismic response of gravity walls.

Louizos Tsantilas, George Gazetas
School of Civil Engineering, National Technical University of Athens, Greece, louizostsantilas@gmail.com

Evangelia Garini
School of Mineral Resources Engineering, Technical University of Crete, Chania, Greece

ABSTRACT: A century has passed since Mononobe (1924) and Okabe (1924) founded the Mononobe–Okabe (M O) method to calculate seismic pressure acting on a gravity wall. The method is still universally used by engineers. In this study, an extensive parametric analysis of a gravity wall subjected to seismic excitation is presented. As excitation we employ a Gabor wavelet with parametrically varying peak acceleration and predominant period T_P. The retaining and foundation soil are homogeneous dry sands, and their cyclic behavior is modeled by employing the constitutive model of Anastasopoulos et al. (2011). The wall–soil interfaces are properly simulated to allow sliding and separation. The induced soil pressure distributions are compared with the M O, the EC8-5 (Lancellotta, 2002, 2007, 2008), the Mylonakis et al. (2007) and the Seed & Whitman (1970) analytical methods.

KEYWORDS: Gravity walls, dry sand, soil pressure, seismic response, Mononobe-Okabe method.

1 INTRODUCTION

One of the main problems in designing a gravity wall in seismic regions is to compute accurately the seismic soil pressures on the wall (Tsantilas et al. 2025).

One century after the seminal contribution of Okabe (1924, 1926), who extended Coulomb's (1776) work to pseudo–statically describe a wall's seismic response, the Mononobe–Okabe (M O; 1924, 1925, 1926, 1929) method remains one of the most popular and influential analytical tools in geotechnical engineering.

Despite its assumptions, it has inspired numerous analytical scientific works exploring various aspects of the Soil Retaining Wall Interaction (Tsantilas 2024), such as those by Kapila (1962), Seed & Whitman (1970), Richards & Elms (1979), Zarrabi (1979), Jacobson (1980), Nadim & Whitman (1983), Al-Homoud & Whitman (1992), Wu & Prakash (2001), Lancellotta (2002, 2007, 2008), Mylonakis et al. (2007), Pender (2019), and many others.

2 SCOPE

2.1 *Main research target*

The main goal of this study is to present—using parametric finite element numerical analyses with Abaqus (2016)—a part of the seismic performance of the simplest and most analyzed form of retaining structure: A rectangular gravity wall that restrains horizontal dry inelastic sand backfill. This wall can also slide and detach from the soil.

2.2 *Secondary research target*

The accuracy of popular M O–type and Rankine–type pseudo–static analytical solutions is explored through comparisons with the numerical results.

3 PARAMETRIC ANALYSES

The numerical analyses are based on the same configuration sketched in Figure 1Figure 1. The height, H, of the wall is taken equal to 12 m (or 6 m), while the width, B, is parametrically varied.

The two wall interfaces with the surrounding soil are characterized by a friction coefficient, μ. The vertical wall interface with backfill soil corresponds to a value of $\mu_1 = 0.384$, whereas the horizontal interface with the foundation soil layer to a parametrically varied coefficient μ_2. The nomenclature is the same as described in Tsantilas et al. (2025).

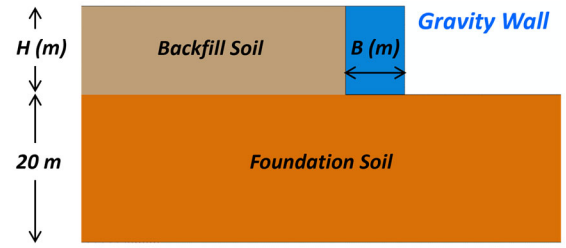

Figure 1. Geometry of the studied problem

The gravity wall with the two-layered soil stratum is excited by idealized Gabor wavelets of varying maximum acceleration amplitude (PGA) and pulse period (T_P). The main values investigated are:

- 0.2 g, 0.4 g, and 0.6 g, for PGA.
- 0.25 s, 0.5 s, and 0.75 s, for T_P.
- 0.333, 0.667, and 1, for μ_2.
- 4 m, 6 m, 8 m, and 10 m for B.

The Gabor pulses used are plotted in Figure 2.

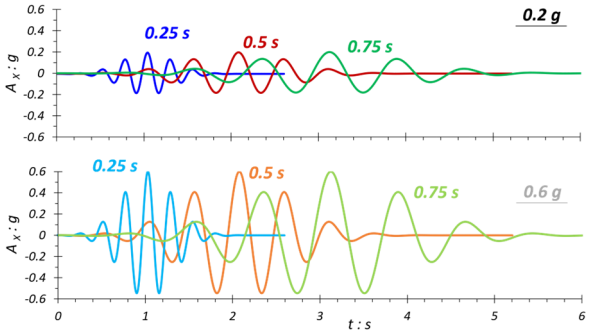

Figure 2. Acceleration–time histories of the Gabor motions (wavelets) used as bedrock excitations.

4 MODEL

Detailed information for the numerical model is given in Tsantilas et al. (2025). Here we focus on the model with the gravity wall of H = 12 m, and B = 8 m, depicted in Figure 3.

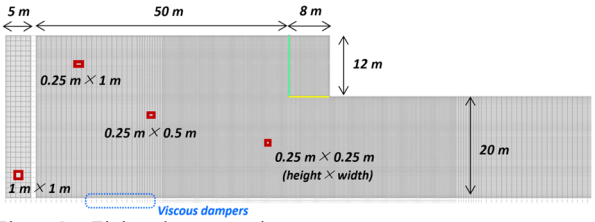

Figure 3. Finite–element mesh.

4.1 *Finite-Element Model*

Wall and soil are modeled by four–node quadrilateral continuous elements, with the soil mesh discretization to be shown in Figure 3. The distance between the wall and the model's boundary is 50 m, to minimize the boundary effects.

Also, to have proper transmission of up–coming waves and to avoid the box effect, a vertical free-field column was introduced on the model side.

Lastly, normal and shear viscous elements ρV_S and ρV_P (per unit area) were utilized at the vertical boundary between the soil domain and the vertical free-field column and at the horizontal boundary between the soil domain and the bedrock to capture radiation damping. The dashpots' coefficients were calculated employing the Dobry & Gazetas (1986) procedure.

4.2 *Materials*

4.2.1 *Concrete wall*

In the current analyses, the wall is assumed to remain elastic with density, $\rho_w = 2.5$ Mg/m^3, Young's modulus of elasticity, $E_w = 25{,}000$ MPa, and Poisson's ratio, $\nu_w = 0.2$.

4.2.2 *Dry dense sand*

Soil properties are presented in Table 1.

Table 1. Soil properties.

		Backfill	Foundation	
Parameter	Symbol	Value	Value	Unit
small-strain average Young's modulus	E_0	100	300	MPA
Poisson's ratio	ν	0.25	0.25	-
soil unit weight	γ	19	19	KN/m^3
soil friction angle	φ	37.5	45	°
parameters of constitutive soil model	a	12,004	14,603	-
	λ	0.1	0.1	-

4.3 *Constitutive soil model*

The numerical analyses performed here utilize the refined plasticity model of Anastasopoulos et al. (2011), as briefly described in Tsantilas (2024, pp. 103/840) and analyzed in Tsantilas et al. (2025). The parameters of this constitutive model for the specific analyses are given in Table 1, for each soil formation. Detailed discussion of the calibration process can be found in Tsantilas et al. (2025), whereas the verification process in Tsantilas et al. (2024).

5 NUMERICAL RESULTS AND DISCUSSION

5.1 *Gravity wall seismic response*

For the sake of brevity, only a minimum of all the parametric results is presented below, for the 12 m × 8 m (H×B) gravity wall with $\mu_2 = 0.667$, excited by 0.2 g and 0.6g Gabor pulses.

Figure 4 illustrates the dimensionless lateral and vertical soil pressure distributions, along the wall's height and base respectively, during the instant of ***maximum soil force*** (***maxF***).

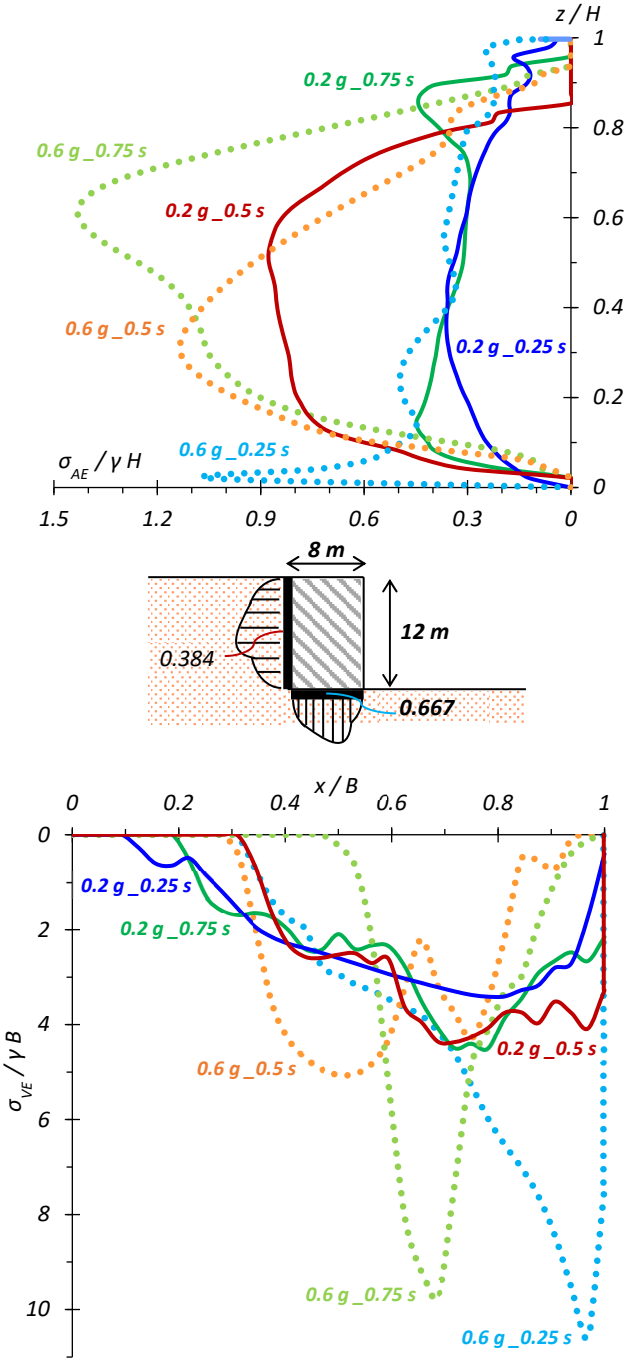

Figure 4. Comparison of dimensionless lateral (top) and vertical (bottom) soil pressure distributions, at the instant of ***maxF***.

Figure 5 and Figure 6 depict the dimensionless lateral and vertical seismic soil pressure profiles, along the wall's height (upper plot) and base (lower plot), during the instants of ***maximum outward wall rotation*** (***maxR***+) and ***minimum lateral soil force*** (***minF***).

All three pressure distributions figures reveal the high variability (in both amplitude and shape) of lateral and vertical earth pressures with the PGA, the dominant period of the Gabor pulse, and with time during shaking (***maxF***, ***maxR***+, ***minF***).

The instants of *maximum* and *minimum lateral soil force* and *maximum outward wall rotation* are the most important time instants where the seismic performance of retaining walls should focus, as explained in Tsantilas et al. (2025) study. The ***maxR***+ and ***minF*** pressures are close to the active pressures, whereas the ***maxF*** are closer to the passive ones.

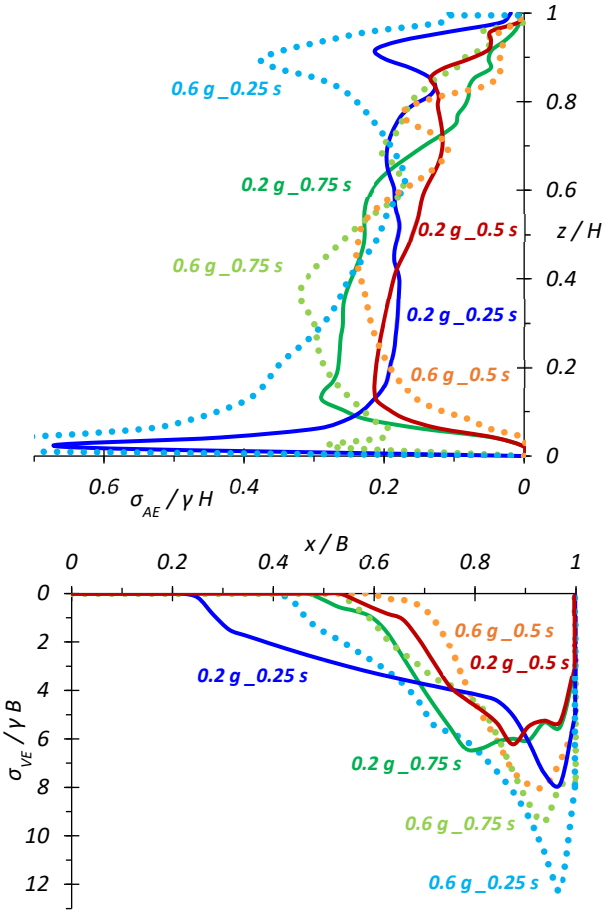

Figure 5. Comparison of dimensionless lateral (top) and vertical (bottom) soil pressure distributions, at the instant of ***maxR***+.

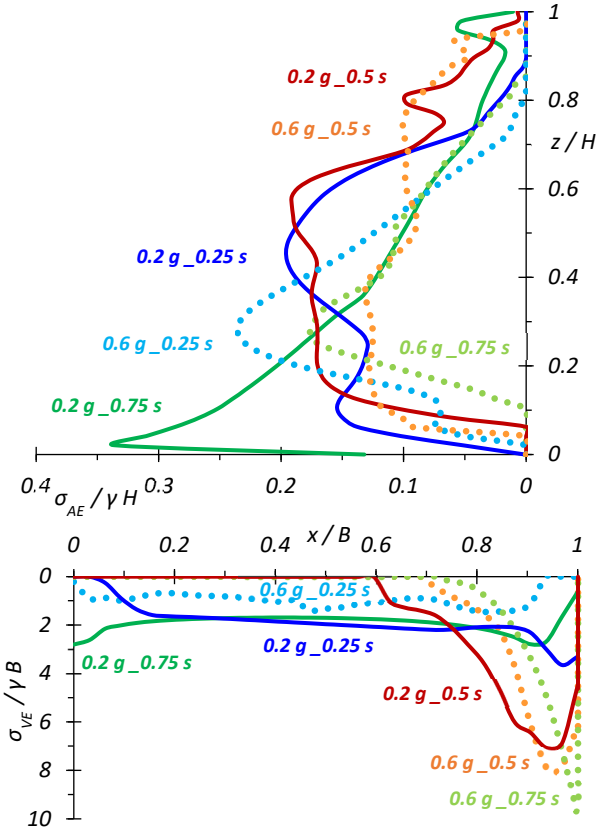

Figure 6. Comparison of dimensionless lateral (top) and vertical (bottom) soil pressure distributions, at the instant of ***minF***.

Figure 7 compares the wall tilt of the 0.2 g and 0.6 g Gabor pulse of $T_P = 0.75$ s in 2-D space, presenting the effect of *PGA* in wall rotation: Higher *PGA* results in greater wall rotation.

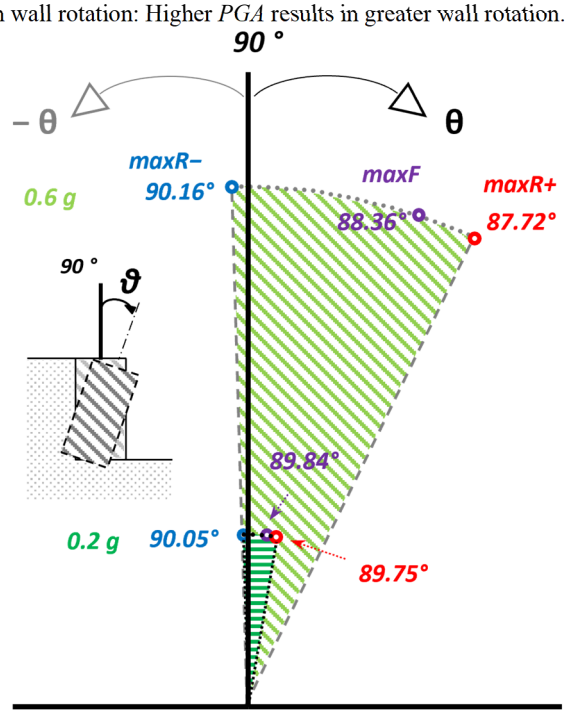

Figure 7. Wall tilt in 2-D space. Points of maximum soil force (***maxF***), maximum outward (***maxR***+) and inward (***maxR-***) rotation for the two *PGA*'s studied [0.2 g (green) and 0.6 g (light green)] and $T_P = 0.75$ s.

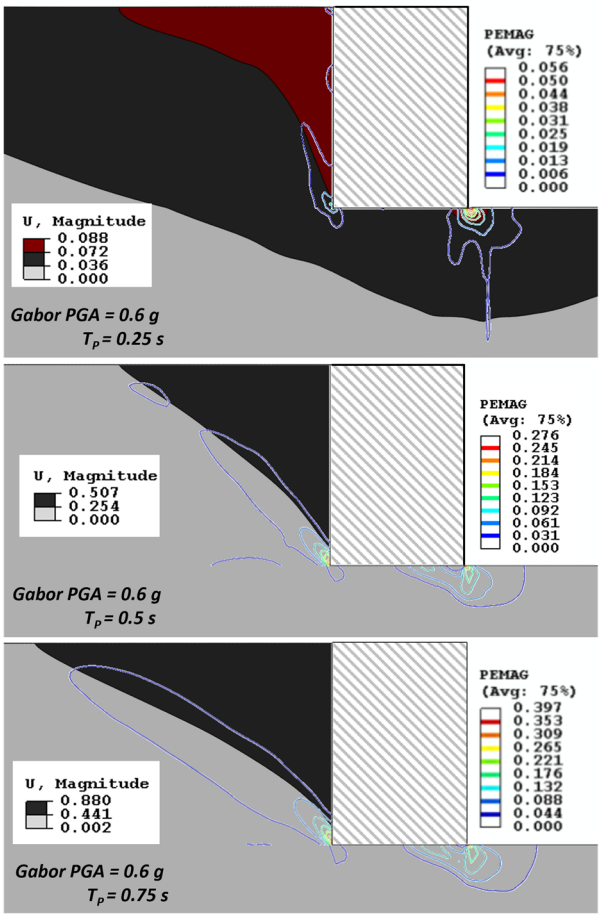

Figure 8. Contours of magnitude displacement and plastic deformation at the end of the analysis with 0.6 g Gabor motion.

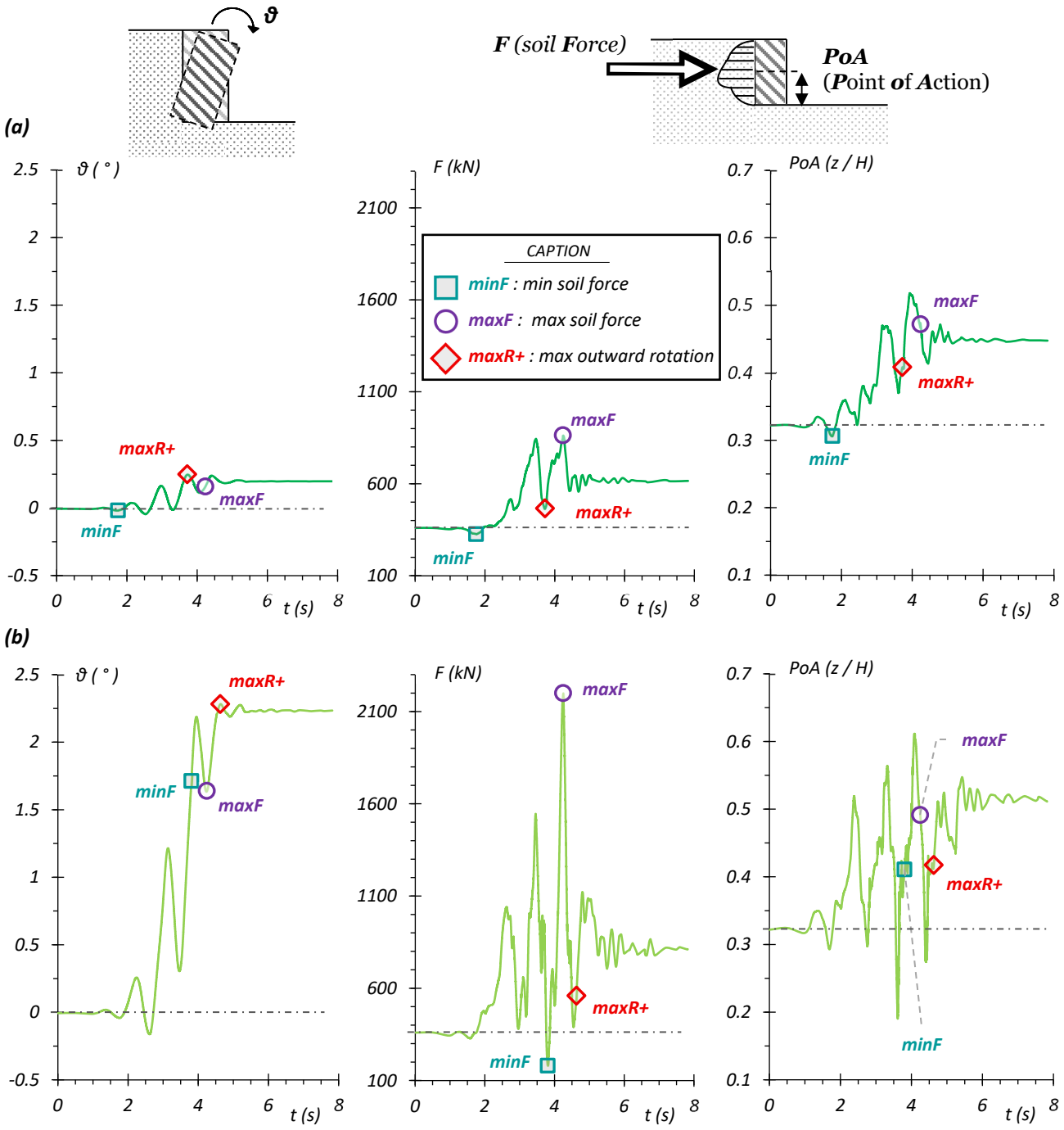

Figure 9. Time histories of wall rotation (left column), lateral soil force (middle), and soil force dimensionless point of action (right), for two different *PGA*'s [0.2 g (**a**; upper plots) and 0.6 g (**b**; lower plots)], but for the same predominant period of the Gabor pulse (T_P = 0.75 s).

Watching carefully Figure 8 the final dimensions of the displacing soil wedge are revealed. Moreover, the low-period pulse of 0.25 s is connected to a different soil–wall response in contrast with the other two pulses of 0.5 s and 0.75 s.

The comparison of the rotational response (Figure 9) from the analyses with the two extreme periods (0.25 s vs 0.75 s) indicates that the low–period pulse shows an almost elastic behavior with an almost tilting response with slight asymmetry, whereas the high–period motion an irreversible asymmetric tilt. This response was also observed by Tsantilas et al. (2025), who explained the phenomenon as a result of resonance between the Gabor period and either the natural period of the foundation soil ($T_{1,fdn} \approx 0.32$ s) or that of the far–field soil ($T_{1,fill} \approx 0.55$ s).

The other two groups of graphs of Figure 9 depict the fluctuation of lateral soil force (in the middle) and point of action (*PoA*) of lateral soil force (at the right) with time. It is obvious that:

- Both parameters vary greatly in time.
- Both parameters take values far higher and lower than their static (at the start of the analysis) values.
- The *PoA* is equal to 1/3 of wall's height (H/3) for only eight times during the 0.75 s motion, and for only one time during the 0.25 s pulse, in contrast with common belief.

5.2 *Numerical results vs analytical methods*

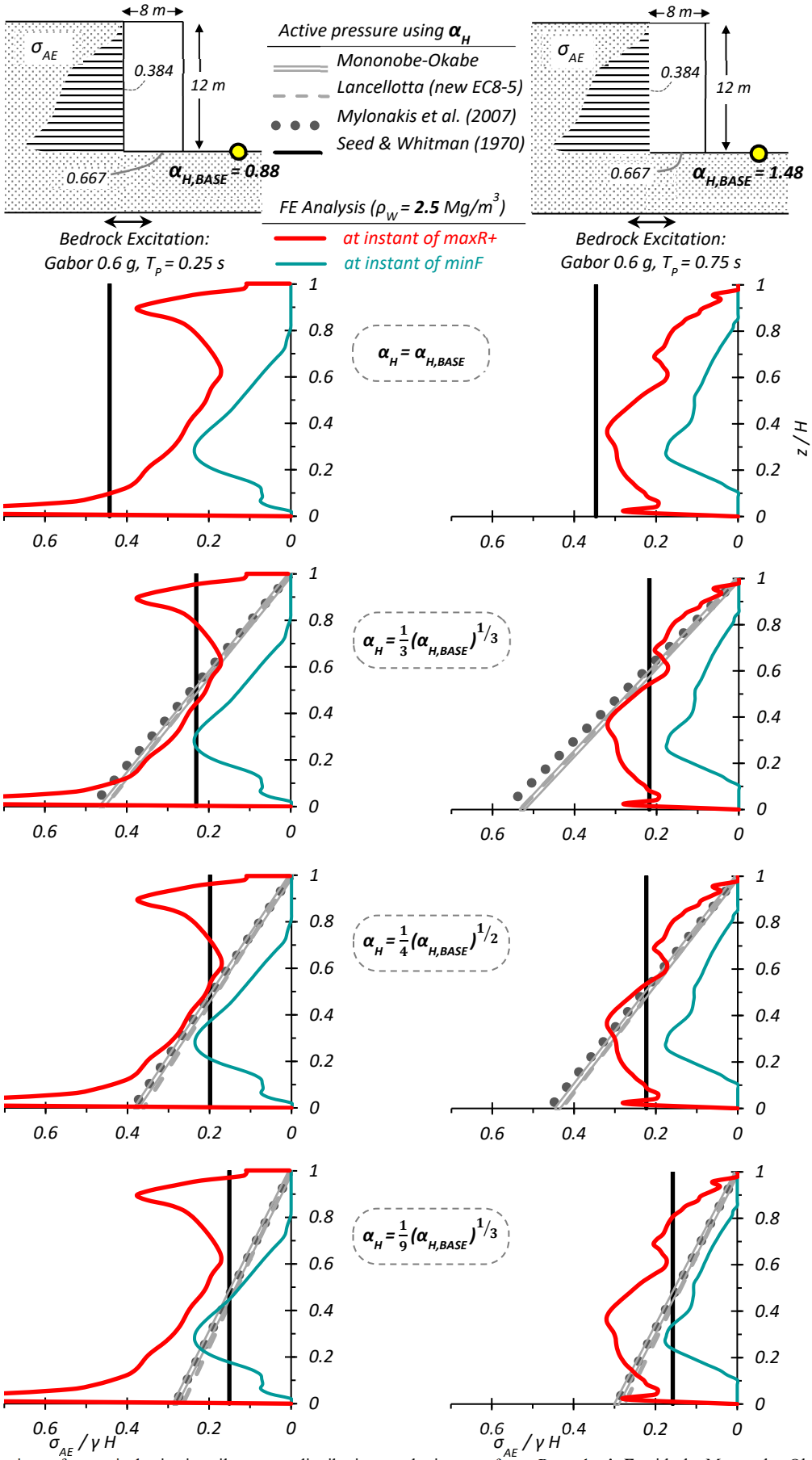

Figure 10. Comparison of numerical seismic soil pressure distributions at the instant of ***maxR+*** and ***minF***, with the Mononobe–Okabe, Lancellotta (new EC8-5), Mylonakis *et al.*, and Seed & Whitman for different definitions of acceleration coefficient.

The numerically calculated profiles of active–type lateral seismic earth pressures (***maxR+***, ***minF***) for two dominant periods of excitation, 0.25 s and 0.75 s, are compared in Figure 10 with the M O active soil pressures, the Seed & Whitman (1970) linear approximation to M O, and two M O–type pseudo–static active soil pressures (Lancellotta–new EC8-5; Mylonakis et al. 2007)). Have in mind that σ_{AE} pressures refer to seismic (total = static + dynamic) pressures.

Observe that the top pressure plots of Figure 10 presents only the comparison of numerical results with the Seed & Whitman approximation, calculated with the equation given in Tsantilas et al. (2025), because the acceleration coefficient in both cases is greater than $\tan\varphi_1 \approx 0.77$ (for purely cohesionless soil) and the M O–type methods do not lead to a solution.

A "proper" value for the seismic horizontal coefficient at the instant of ***maxR+*** could be computed with the Noda et al. (1975) equation and the Tsantilas et al. (2025) proposal pictured in the 2nd and 3rd line of Figure 10 respectively. For the case of ***minF***, the use of Equation (1) proposed in Tsantilas (2024) results in a very close solution for both dominant periods.

$$\alpha_H = \frac{1}{9}(\alpha_{H,BASE})^{1/3} = \frac{1}{9}\left(\frac{PGA}{g}\right)^{1/3} \quad (1)$$

6 CONCLUSIONS

6.1 *Summary*

This study has shed new light on critical parameters influencing the seismic performance of retaining walls, thereby clarifying previously ambiguous aspects of Soil–Wall Interaction under dynamic loading. More specifically:

- The seismic pressures on the wall are changing with time during a motion.
- The point of action of lateral soil force is constantly varying over time.
- The frequency content of the excitation plays a significant role to the overall seismic response of the soil wedge–retaining wall system, along with the intensity of the motion.
- The pseudo–static Mononobe–Okabe–type analytical methods paired with the appropriate horizontal acceleration coefficient equation could adequately predict the amplitude of seismic lateral active pressures.

6.2 *Conclusion*

Although a century has passed since Okabe's (1924, 1926) groundbreaking work, our numerical analysis—employing appropriate finite elements to realistically model the seismic response—suggests that the M O method will remain in use for at least another century, provided that the horizontal acceleration coefficient is properly defined through suitable equations.

7 REFERENCES

Al-Homoud, A.S., and Whitman, R.V. 1992. Evaluating tilt of gravity retaining walls during earthquakes. *Proc. of the 10th World Conference on Earthquake Engineering*, Madrid, Spain, vol. III, Session 6.3, 1683-1688.

Anastasopoulos, I., Gelagoti, F., Kourkoulis, R., and Gazetas, G. 2011. Simplified constitutive model for simulation of cyclic response of shallow foundations: validation against laboratory tests. *J. Geotech. Geoenviron. Engng, ASCE* 137(12), 1154-1168, http://doi.org/10.1061/(ASCE)GT.1943-5606.0000534.

Abaqus, 2016. *Documentation*. Providence, RI, USA: Dassault Systèmes Simulia Corp.

Coulomb, C.A. 1776. Essai sur une application des regles de maximis et minimis quelques problemes de statique, relatits a l'architecture. *Memoires de Mathematique de l'Academie Royale de Science* 7, 343-387.

Dobry, R., and Gazetas, G. 1986. Dynamic response of arbitrarily–shaped foundations. *J. Geotech. Engng, ASCE* 113(2), 109-135.

European Committee for Standardization, 2022. *EC8 - Part 5: Geotechnical Aspects, Foundations, Retaining and Underground Structures – DRAFT prEN 1998-5, September edition*. Brussels: CEN.

Jacobson, P.N. 1980. Translational behavior of gravity retaining walls during earthquakes. *Research Report 80-9*, University of Canterbury, New Zealand.

Kapila I.P. 1962. Earthquake resistant design of retaining walls. *Proc. of 2nd Symposium on Earthquake Engineering*, School of Research and Training in Earthquake Engineering, University of Roorkee, India, 97-107.

Lancellotta, R. 2002. Analytical solution of passive earth pressure. *Géotechnique* 52(8), 617-619, https://doi.org/10.1680/geot.2002.52.8.617.

Lancellotta, R. 2007. Lower–bound approach for seismic passive earth resistance. *Géotechnique* 57(3), 319-321, https://doi.org/10.1680/geot.2007.57.3.319.

Lancellotta, R. 2008. The collapse of soil structures. In: *Geotechnical Engineering*, Zanichelli Ed, Taylor & Francis e–Library, 2nd edition.

Mononobe, N. 1924. Discussion and consideration on vertical earthquake motion. *Proc. JSCE* 10(5), 1063-1095 (in Japanese).

Mononobe, N. 1925. Design of a seismic gravity wall. Report of Kantō Earthquake Damages of 1923. *Proc. JSCE* 3 (in Japanese).

Mononobe, N. 1929. Earthquake–Proof construction of masonry dams. *Proc. of World Engineering Congress*, Tokyo, Japan, 9, 275-278.

Mononobe, N., and Matsuo, H. 1929. On the determination of earth pressure during earthquake. *Proc. of World Engineering Congress*, Tokyo, Japan, 9(388), 177-185.

Mylonakis, G., Kloukinas, P., and Papantonopoulos, C. 2007. An alternative to the Mononobe–Okabe equations for seismic earth pressures. *Soil Dyn. Earthq. Engng* 27(10), 957-969, https://doi.org/10.1016/j.soildyn.2007.01.004.

Nadim, F., and Whitman, R.V. 1983. Seismically induced movement of retaining walls. *J. Geotech. Engng* 109(7), 915-931, https://doi.org/10.1061/(ASCE)0733-9410(1983)109:7(915).

Noda, S., Uwabe, T., and Chiba, T. 1975. *Relation between seismic coefficient and ground acceleration for gravity quay wall*. Report Subject *3* 14(4), 67-111, P.H.R.I. Ministry of Transport, Nagase, Yokosuka, Japan (in Japanese).

Okabe, S. 1924. General theory on earth pressure and seismic stability of retaining wall and dam. *J. Japan Soc. Civ. Engrs* 10(6), 1277-1323.

Okabe, S. 1926. General theory of earth pressures. *J. Japan Soc. Civ. Engrs* 12(1), 123-134 (in Japanese).

Pender, M.J. (2019). Foundation design for gravity retaining walls under earthquake. *Proc Instn Civ. Engrs– Geotech. Engng* 172, No.1, 42-54, https://doi.org/10.1680/jgeen.17.00233.

Richards, R., and Elms, D.G. 1979. Seismic behavior of gravity retaining walls. *J. Geotech. Engng Div.* 105(GT 4), 449-464, https://doi.org/10.1061/AJGEB6.0000783.

Seed, H.B., and Whitman, R.V. 1970. Design of earth retaining structures for dynamic loads. *Proc. of the ASCE Specialty Conference on Lateral Stresses in the Ground and Design of Earth–Retaining Structures*, Ithaca, New York, 1, 103-147.

Tsantilas, L. 2024. *Seismic response of displacing and non–displacing retaining systems: New insights*. Doctoral thesis, NTUA, Athens, Greece, thesis.ekt.gr/58492?lang=el.

Tsantilas, L., Garini, E., and Gazetas, G. 2024. Seismic response of retaining walls: Theoretical parametric insights after centrifuge validation. *Soil Dyn. Earthq. Engng* 176, 108314, https://doi.org/10.1016/j.soildyn.2023.108314.

Tsantilas, L., Garini, E., and Gazetas, G. 2025. Insight into the seismic response of gravity retaining walls. *Géotechnique* (in press), https://doi.org/10.1680/jgeot.24.01063.

Wu, Y., and Prakash, S. 2001. Seismic displacement of rigid retaining walls—state of the art. *Proc. of the 4th International Conference on Recent Advances in Geotechnical Earthquake Engineering and Soil Dynamics*, San Diego, CA, 7.05.

Zarrabi, K. 1979. *Sliding of gravity retaining wall during earthquakes considering vertical acceleration and changing inclination of failure surface*. Master thesis, MIT, Cambridge, Massachusetts.